Supporting Information

3D Nanoporous $Co_9S_4P_4$ Pentlandite as a Bifunctional Electrocatalyst for Overall Neutral Water Splitting

Yongwen Tan, [†‡] Min Luo, [§] Pan Liu, [£] Chun Cheng, [‡] Jiuhui Han, [‡] Kentaro Watanabe, [‡] and Mingwei Chen[*‡¶⊥]

†School of Materials Science and Engineering, Hunan University, Changsha 410082, China

‡ Advanced Institute for Materials Research, Tohoku University, Sendai 980-8577, Japan

§ Department of Physics, Shanghai Second Polytechnic University, Shanghai 201209, China

£ State Key Laboratory of Metal Matrix Composites, School of Materials Science and Engineering, Shanghai Jiao Tong University, Shanghai 200030, China

¶ CREST, JST, 4-1-8 Honcho Kawaguchi, Saitama 332-0012, Japan

⊥ Department of Materials Science and Engineering, Johns Hopkins University, Baltimore, MD 21214, USA

*Correspondence to: mwchen@jhu.edu

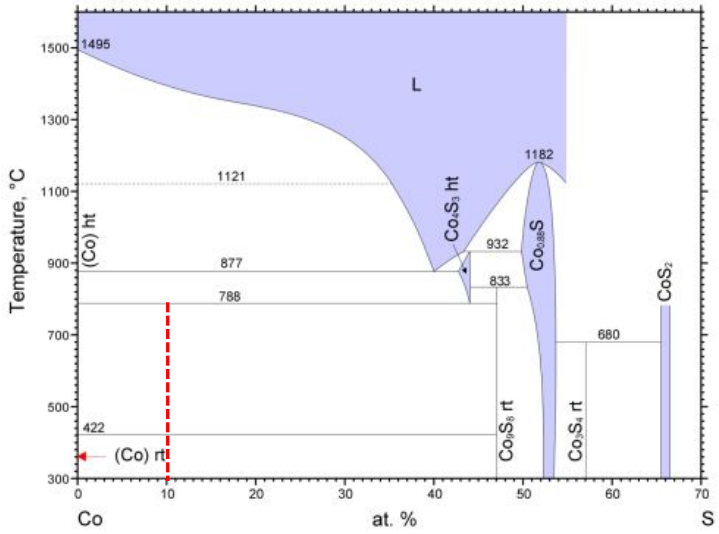

Figure S1. The binary Co-S phase diagram (Cited from NIMS Materials data)**,** showing the phase constitution information of the Co and Co_9S_8 phases ($0 \leq S\% \leq 47\%$, at%). The red dash line indicates the nominal composition of the rapidly quenched Co_9S_8 ribbons.

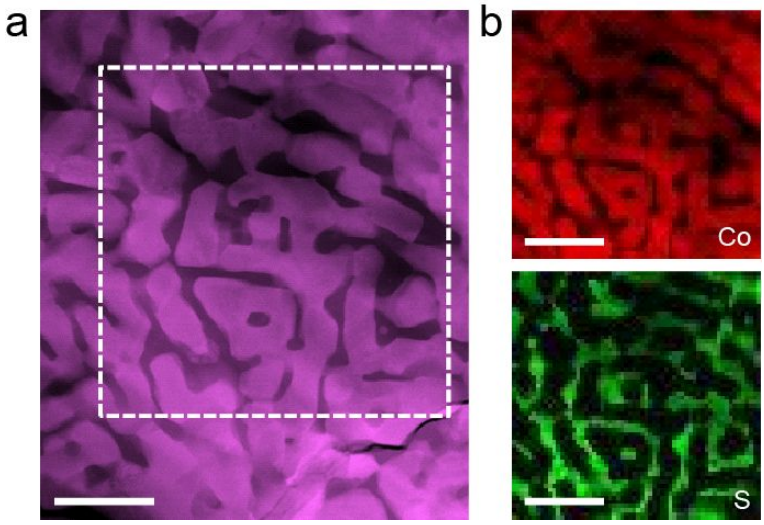

Figure S2. TEM characterization of a rapidly-solidified $Co_{90}S_{10}$ precursor ribbons. (a) High-angle annular dark-field scanning TEM image of the rapidly-solidified two-phase alloy. The marked box is the selected region for EDS chemical analysis. (b) STEM EDS element mappings of the alloy taken from the marked region in (a). Scale bars: (a) and (b) 100 nm.

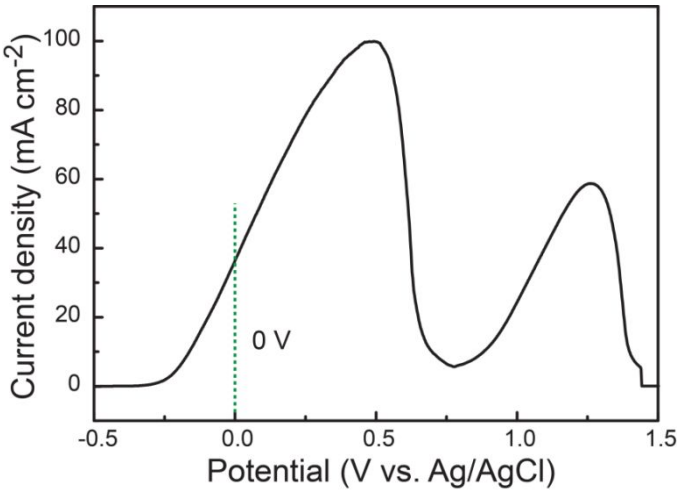

Figure S3. The linear sweep voltammetry (LSV) curve of the $Co_{90}S_{10}$ ribbons in 0.5 M HCl. There are two distinct peaks corresponding to the oxidation (or dissolution) of the Co and Co_9S_8 phases, respectively. The critical dissolution potential of the Co phase is ~-0.2 V vs. Ag/AgCl while it is ~0.75 V for the dissolution of the metal sulfide. In this study we selected the corrosion potential of 0 V for the selective dissolution of the Co phase at which the Co_9S_8 phase is safe.

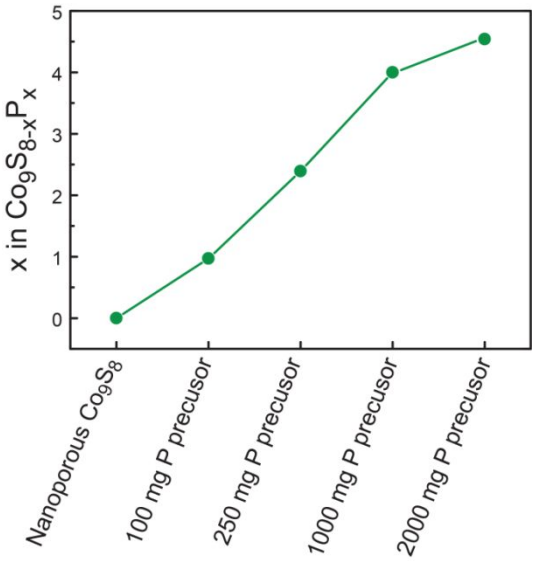

Figure S4. The correlation of P content in $Co_9S_{8-x}P_x$ with the loading mass of NaH_2PO_2 precursor. The P content in the np-$Co_9S_{8-x}P_x$ increased with increasing NaH_2PO_2 precursor dosage used in the synthesis until 50% of S was substituted with P (x=4 for $Co_9S_{8-x}P_x$). Further increase of the P dosage could slightly increase the P/S ratio in np-$Co_9S_{8-x}P_x$.

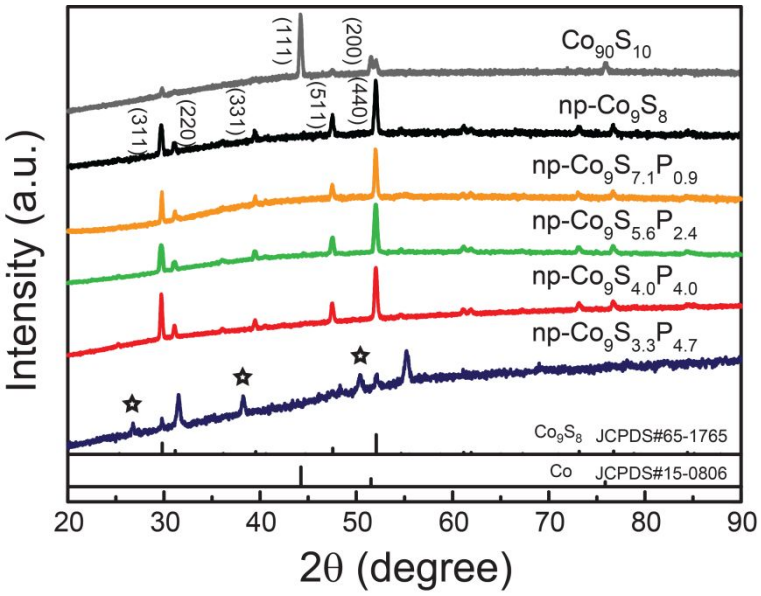

Figure S5. XRD spectra of the precursor Co_9S_8 ribbons, np-Co_9S_8 and np-$Co_9S_{8-x}P_x$. After complete dissolution of the Co phase, the np-Co_9S_8 phase was retained. The P substitution does not cause detectable structure changes until the P content increases to x=4.7 while a new Co_3S_4 phase appears with the diffraction peaks marked by *.

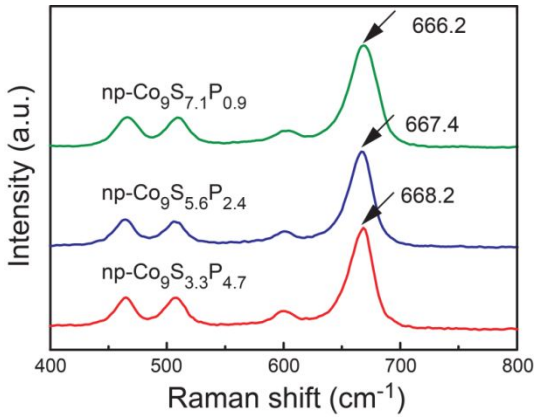

Figure S6. Raman spectra of np-$Co_9S_{8-x}P_x$, x = 0.9, 2.4, and 4.7.

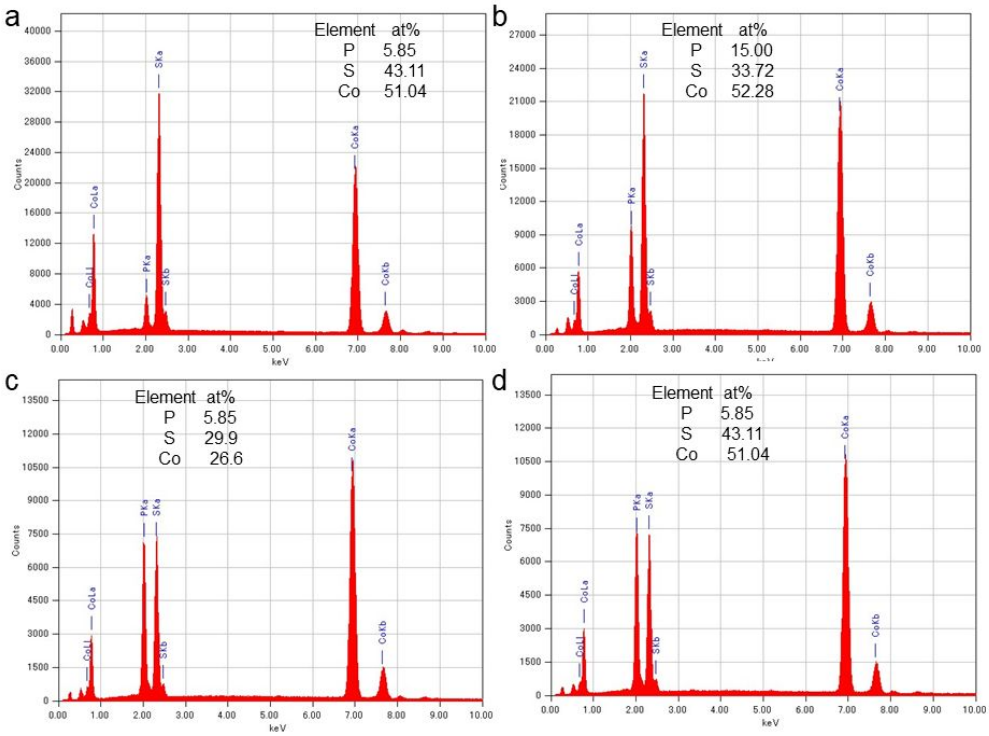

Figure S7. EDS spectra of np-$Co_9S_{8-x}P_x$ with different S/P ratios.

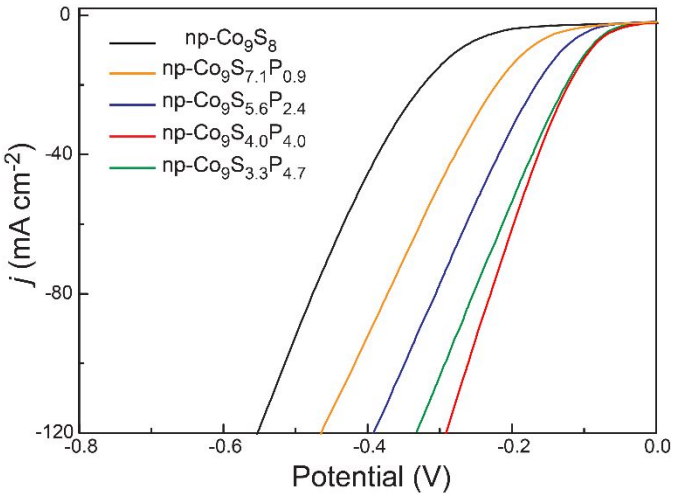

Figure S8. Original HER polarization curves without iR-correction of np-$Co_9S_{8-x}P_x$ in neutral solution.

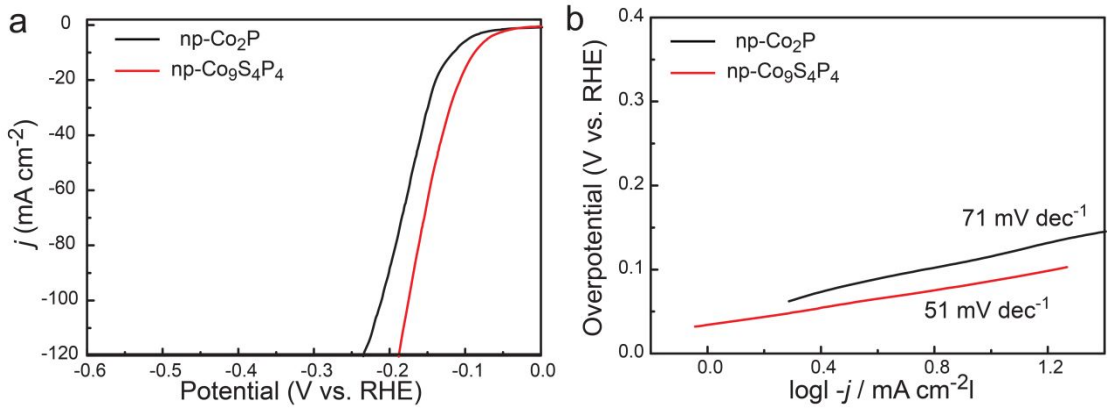

Figure S9. Comparison of HER performance between np-Co_2P and np-$Co_9S_4P_4$ in 1.0 M PBS. (a) Polarization curves, (b) corresponding to Tafel slope.

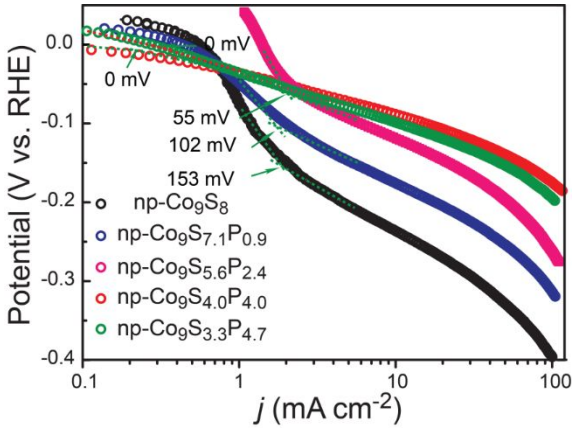

Figure S10. Onset potentials of np-Co_9S_8 and np-$Co_9S_{8-x}P_x$ with different S/P ratios in 1.0 M PBS.

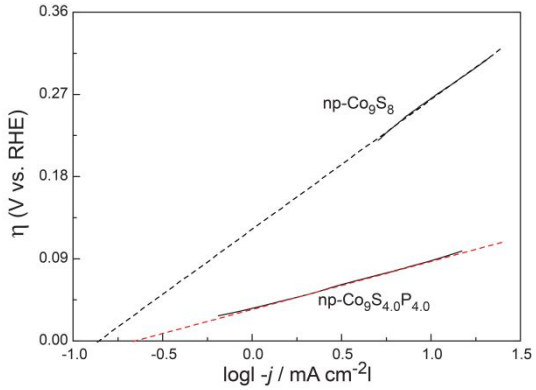

Figure S11. Calculated exchange current densities of np-Co_9S_8 and np-$Co_9S_4P_4$ catalyst by applying extrapolation method to the Tafel plots

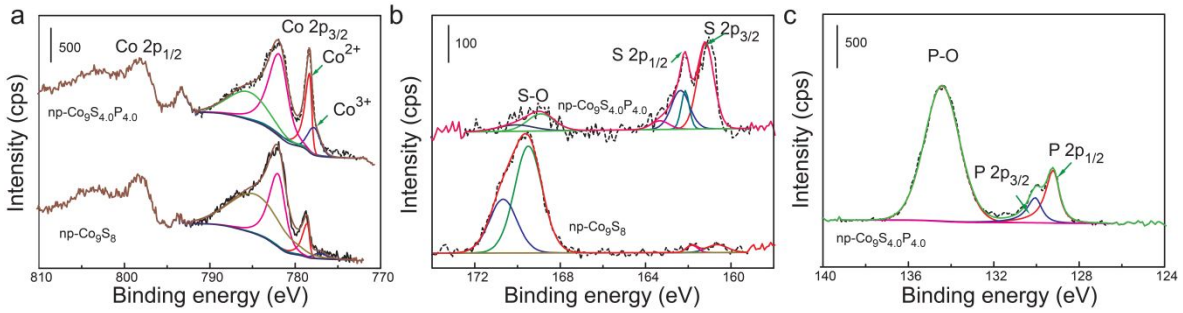

Figure S12. XPS spectra of np-$Co_9S_4P_4$ after long-term HER testing in neutral solution. (a) Co 2p, (b) S 2p, and (c) P 2p region. As the figure shown, the np-$Co_9S_4P_4$ electrode can retain the intrinsic feature after long-term HER testing. The negligible sulfate peaks were observed in the Figure S12b. However, the sulfate peaks are obvious increased form pristine np-Co_9S_8 electrode. The results clearly verified that it is indeed the P substitution renders the excellent catalytic durability.

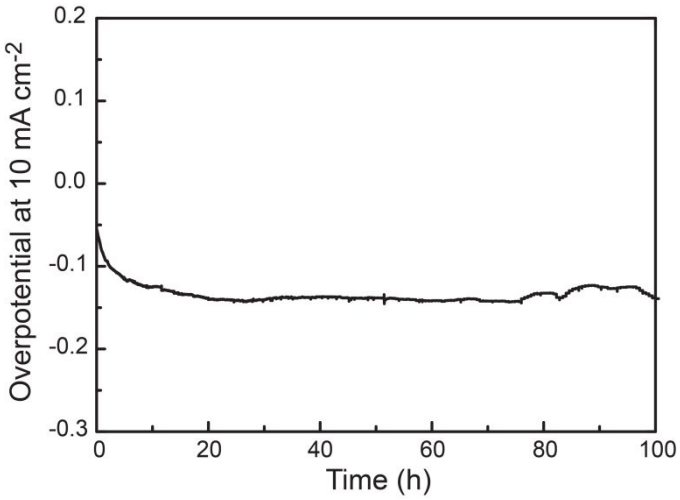

Figure S13. Long time catalytic stability of the np-$Co_9S_4P_4$ electrode. Constant current density of 10 mA cm^{-2} was employed to drive continuous hydrogen evolution reaction. The fluctuation of voltage in the catalytic process may be caused by H_2 bubbles.

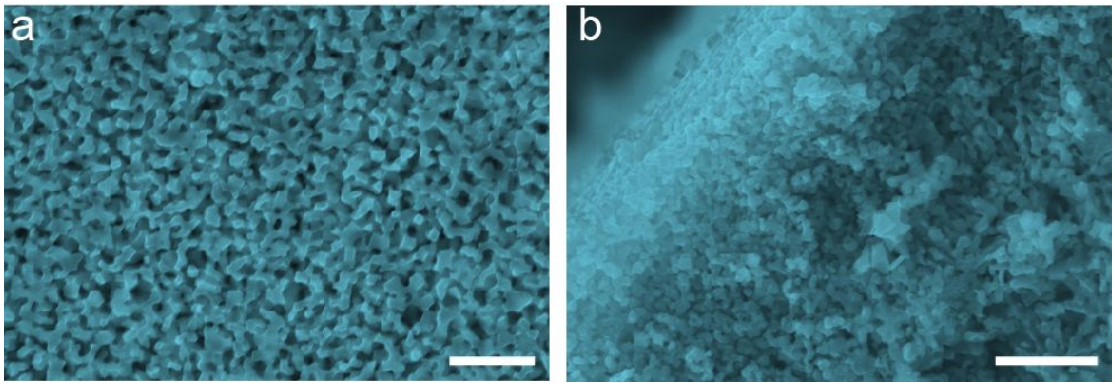

Figure S14. SEM images of self-support np-$Co_9S_4P_4$ electrode after long-term testing. (a) Face section, (b) cross section. Scale bars: (a) 500 nm, (b) 1 μm

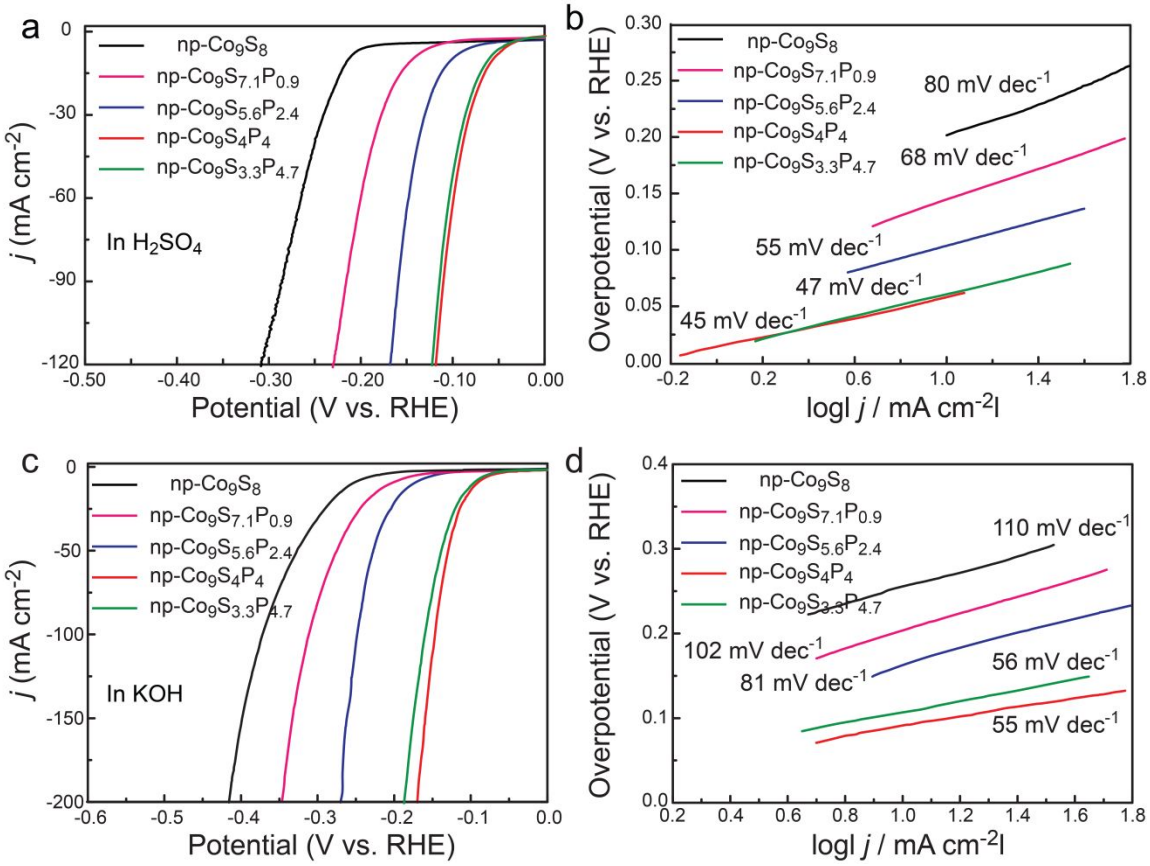

Figure S15. HER performances of np-$Co_9S_{8-x}P_x$ with different P/S ratios in acidic and basic solutions. (a) Polarization curves in 0.5 M H_2SO_4 and (b) corresponding to Tafel slope. (c) Polarization curves in 1.0 M KOH and (d) corresponding to Tafel slope.

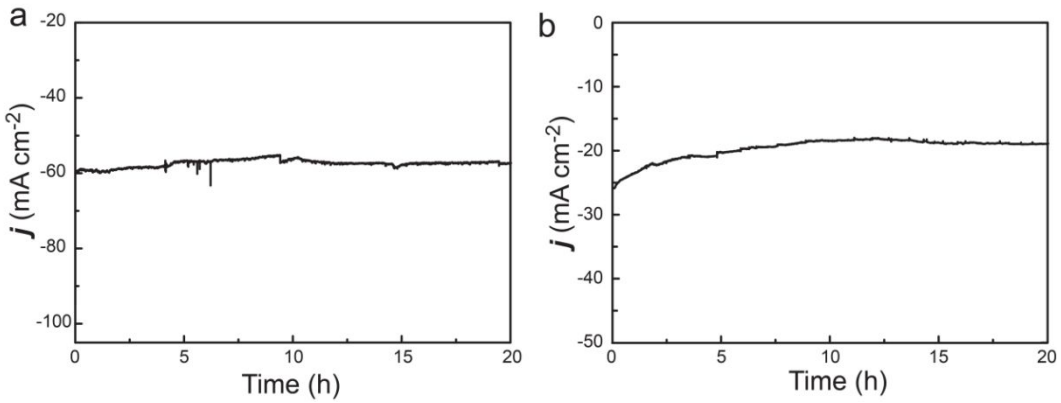

Figure S16. Chronoamperometric response recorded on np-$Co_9S_4P_4$ electrode in (a) the acidic solution and (b) basic solution at a constant overpotential of -100 mV and -150 mV, respectively

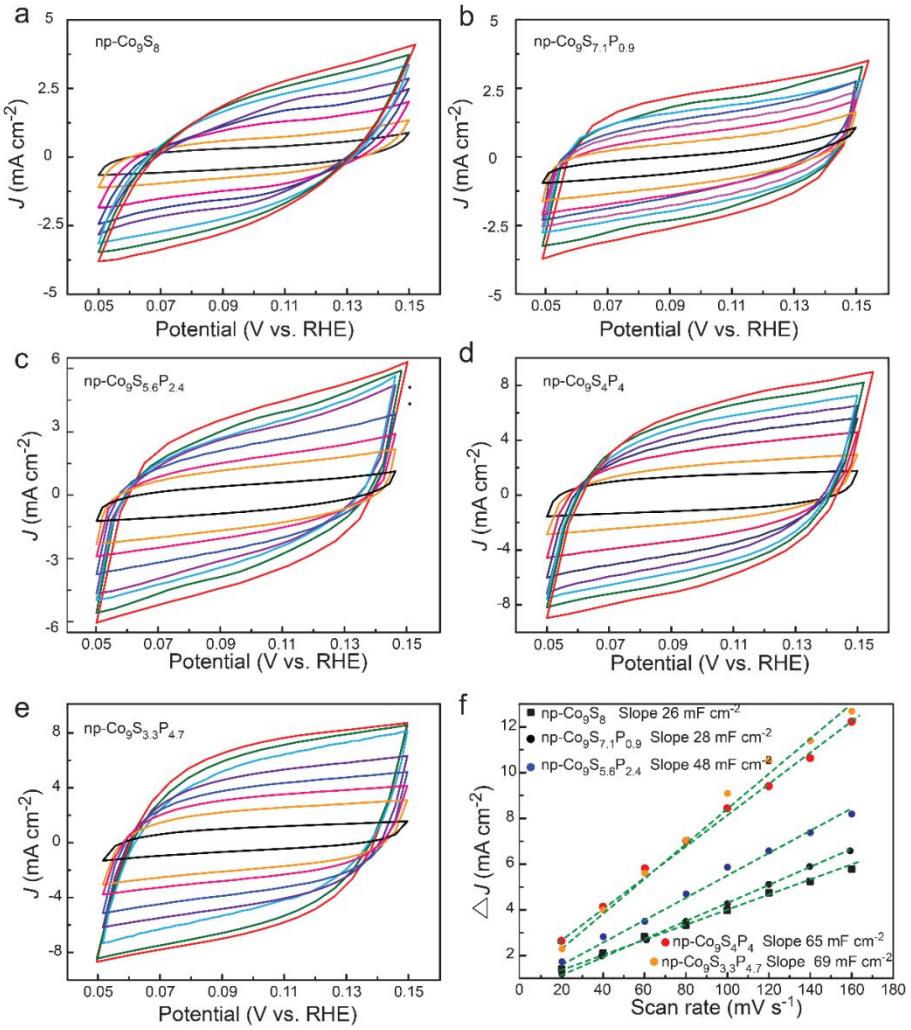

Figure S17. (a-e) Cyclic voltammograms (CVs) of np-$Co_9S_{8-x}P_x$. The CVs were measured at various scan rates (20, 40, 60, 80, 100, 120, 140 and 160 mV/s) from -0.05 to -0.15 V vs RHE. (f) The plots of current densities against scan rates. Δj is the difference between anodic and cathodic current densities at a potential of 0.10 V vs RHE.

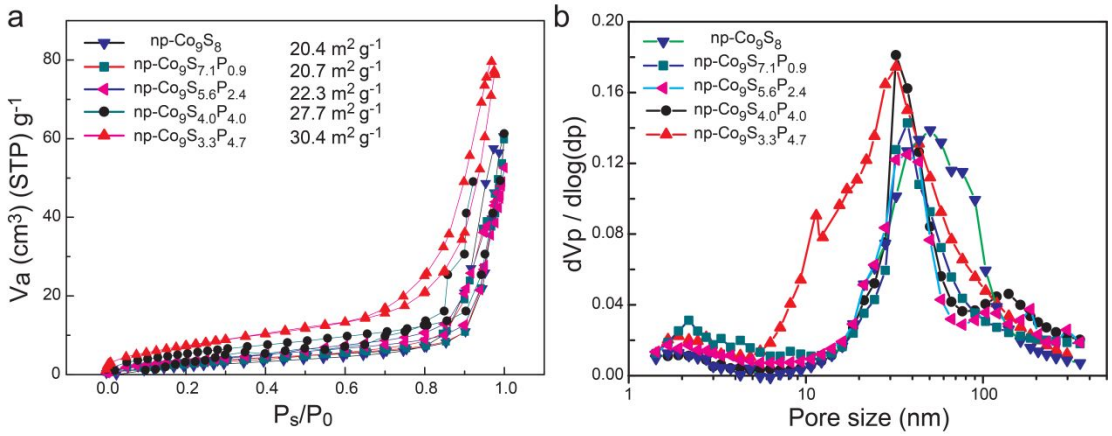

Figure S18. (a) N_2 adsorbing-desorbing isotherm curves of np-Co_9S_8 and np-$Co_9S_{8-x}P_x$. (b) The pore size distribution of as-prepared np-Co_9S_8 and np-$Co_9S_{8-x}P_x$.

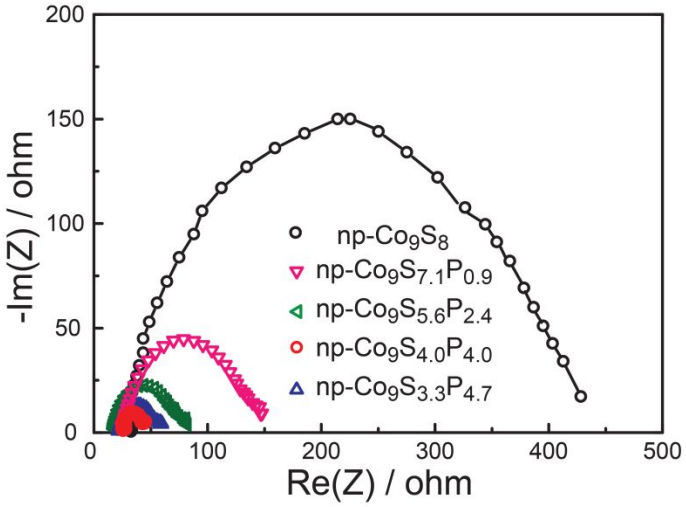

Figure S19. Electrochemical impedance spectroscope (EIS) Nyquist plots of np-Co_9S_8 and np-$Co_9S_{8-x}P_x$ with different P/S ratios in 1.0 M PBS.

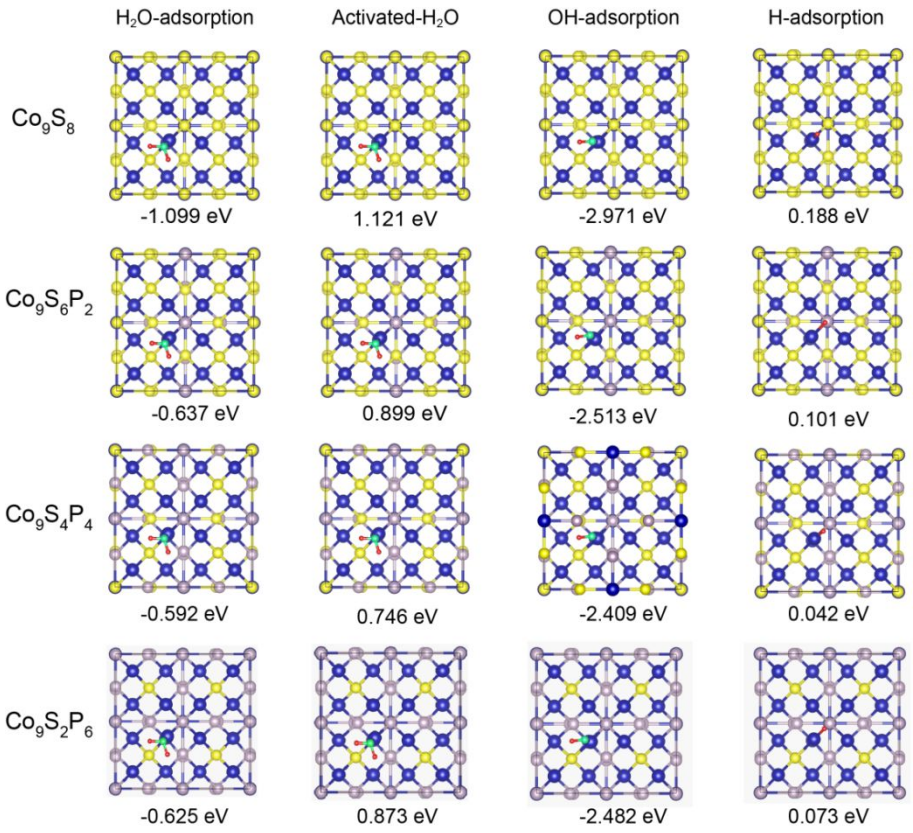

Figure S20. The calculated free energies of H_2O adsorption, activated H_2O adsorption, OH adsorption and H adsorption of $Co_9S_{8-x}P_x$ with different P/S ratios.

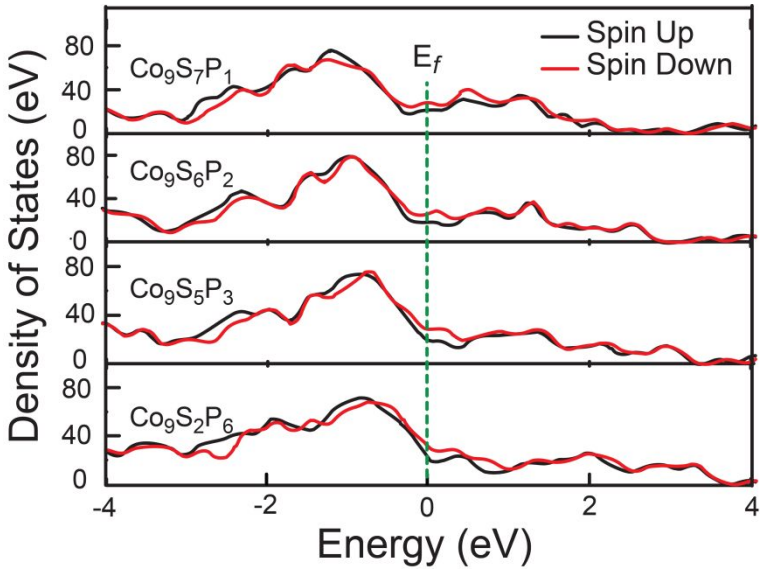

Figure S21. Spin resolved projected density of states (PDOS) for np-$Co_9S_{8-x}P_x$ obtained from DFT calculations. As the P concentration increases, the occupied states of electrons increase around Fermi level and thus the conductivity of np-$Co_9S_{8-x}P_x$ becomes better.

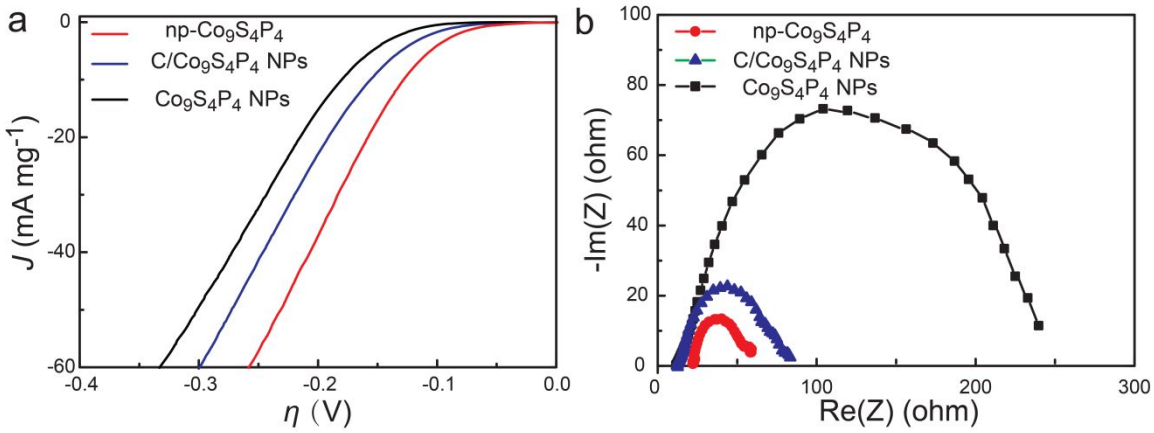

Figure S22. (a) Comparison on HER activities of self-supported np- $Co_9S_4P_4$ electrode， $C/Co_9S_4P_4$ nanoparticles (NPs) loaded on glassy carbon ($C/Co_9S_4P_4$ NPs/GC), and $Co_9S_4P_4$ nanoparticles loaded on glassy carbon ($Co_9S_4P_4$ NPs/GC) in 1.0 M PBS. (b) Nyquist plots of self-supported np-$Co_9S_4P_4$, $C/Co_9S_4P_4$ NPs/GC, $Co_9S_4P_4$ NPs/GC in 1.0 M PBS at an overpotential of -100 mV. The Nyquist plots show that the arc radius of self-supported np-$Co_9S_4P_4$ is obviously smaller than that of $C/Co_9S_4P_4$ NPs/GC and $Co_9S_4P_4$ NPs/GC, suggesting lower solid state interface layer resistance and charge transfer resistance of the bicontinuous nanoporous catalyst.

Table S1. HER performances of np-$Co_9S_{8-x}P_x$ and other high-performance noble-metal-free electrocatalysts in neutral electrolytes. (j: current density; η: overpotential; η_0: onset potential)

Catalysts	Substrate	electrolyte	η_0 (mV)	j (mA cm^{-2})	η（mV）at the corresponding j	Tafel slope (mV dec^{-1})	Reference
np-$Co_9S_4P_4$	Free-standing	1 M PBS	0	10	87	52	This work
np-Co_9S_8	Free-standing	1 M PBS	153	10	264	118	This work
H_2-CoCat/FTO	FTO	0.5 M PBS	50	2	385	140	Ref. 1
Co-S/FTO	FTO	1 M PBS	43	10	~160	93	Ref. 2
CoP nanowire array	carbon cloth	0.2 M PBS	N/A	10	106	93	Ref. 3
CoP nanosheets	Ti plate	0.2 M PBS	N/A	10	149	58	Ref. 4
FeP nanorod array	carbon cloth	0.2 M PBS	112	10	202	71	Ref. 5
FeP nanoparticles	Ti plate	1 M PBS	N/A	10	102	N/A	Ref. 6
WP_2	GCE*	1 M PBS	60	10	244	92	Ref. 7
MoP nanosheet	Carbon flake	1 M PBS	N/A	1	300	77.8	Ref. 8
Carbon-armored Co_9S_8 nanoparticle	GCE	1 M PBS	150	10	280	N/A	Ref. 9
Co-NRCNTs	GCE	1 M PBS	~250	10	540	N/A	Ref. 10
CoN_X-C	GCE	1 M PBS	30	10	247	N/A	Ref. 11
Ni_3S_2 sheet	Ni Foam	1 M PBS	N/A	10	170	N/A	Ref. 12
Ni-S	FTO*	PBS (concertrat	237	10	337	77	Ref. 13

		ion not mentioned)					
Amorphous MoS_3	GCE	PBS (concertration not mentioned)	N/A	2	280	86	Ref. 14
NPG@/$MoS_{2.7}$	GCE	0.2 M PBS	N/A	1	250	60	Ref. 15
Ni-Mo-S	Carbon fiber	0.5 M PBS	132	10	200	85.3	Ref. 16
MoS_2/N-doped graphene nanosheet aerogel	GCE	100 mM PBS	N/A	10	175	230	Ref. 17
$CuMoS_4$	GCE	0.1 M PBS	~550	2	210	N/A	Ref. 18
Mo_2C@NC	GCE	0.1 M PBS	N/A	10	156	N/A	Ref. 19
f-MWCNTs @Pd/TiO2	GCE	0.1 M PBS	N/A	1	170	130	Ref. 20

*GCE: glass carbon electrode; FTO: fluorine-doped tin oxide

Table S2. HER performances of np-$Co_9S_4P_4$ and other high-performance noble-metal-free electrocatalysts in acidic electrolytes. (j: current density; η: overpotential; η_0: onset potential)

Catalysts	Substrate	electrolyte	η_0 (mV)	η（mV）at j=10 mA cm^{-2}	Tafel slope (mV dec^{-1})	Reference
np-$Co_9S_4P_4$	Free-standing	0.5 M H_2SO_4	~0	58	45	This work
np-Co_9S_8	Free-standing	0.5 M H_2SO_4	~150	216	80	This work
CoS_2 film	GCE*	0.5 M H_2SO_4	N/A	232	44.6	Ref. 21
$Co_{0.32}Ni_{0.68}S_2$ film	GCE	0.5 M H_2SO_4	N/A	276	66.3	Ref. 21
$Fe_{0.43}Co_{0.57}S_2$ film	GCE	0.5 M H_2SO_4	N/A	192	55.9	Ref. 21
$Co_{0.56}Ni_{0.44}Se_2$ film	GCE	0.5 M H_2SO_4	N/A	252	49.7	Ref. 21
$CoSe_2$/CP	Carbon fiber	0.5 M H_2SO_4	N/A	137	42.1	Ref. 22
CoS_2/rGO/CNTs	GCE	0.5 M H_2SO_4	N/A	143	51	Ref. 23
$Fe_{0.9}Co_{0.1}S_2$/CNT	GCE	0.5 M H_2SO_4	N/A	160	46	Ref. 24
CoS_2 nanowires	GCE	0.5 M H_2SO_4	N/A	145	51.6	Ref. 25
Double-gyroid MoS_2	FTO*	0.5 M H_2SO_4	N/A	~220	50	Ref. 26
Co_2P NPs	GCE	0.5 M H_2SO_4	N/A	95	45	Ref. 27
Porous Co-based film	Au film	0.5 M H_2SO_4	35	150	53	Ref. 28
CoP	Ti foil	0.5 M H_2SO_4	N/A	N/A	50	Ref. 29
CoP	Carbon cloth	0.5 M H_2SO_4	38	75	51	Ref. 3

CoP/CNT	GCE	0.5 M H_2SO_4	40	122	54	Ref. 30
CoP	Ti foil	0.5 M H_2SO_4	40	90	43	Ref. 4
Ni_2P NPs	GCE	0.5 M H_2SO_4	>50	117	46	Ref. 31
Cu_3P NW	Carbon fiber	0.5 M H_2SO_4	62	143	67	Ref. 32
MoP	GCE	0.5 M H_2SO_4	40	125	54	Ref. 33
P-WC/RGO	GCE	0.5 M H_2SO_4	46	85	54	Ref. 34
Porous Mo_2C	GCE	0.5 M H_2SO_4	25	142	53	Ref. 35
Co-NRCNT	GCE	0.5 M H_2SO_4	50	260	69	Ref. 10
Mo phosphosulfide	GCE	0.5 M H_2SO_4	N/A	86	50	Ref. 36
CoPS NP|s	Ti foil	0.5 M H_2SO_4	∼0	48	56	Ref. 37
$MoS_{2(1-x)}P_x$	GCE	0.5 M H_2SO_4	N/A	~150	57	Ref. 38

*GCE: glass carbon electrode; FTO: fluorine-doped tin oxide

Table S3. HER performances of np-$Co_9S_4P_4$ and other high-performance noble-metal-free electrocatalysts in basic electrolytes (j: current density; η: overpotential; η_0: onset potential).

Catalysts	Substrate	electrolyte	η_0 (mV)	η（mV）at j=10 mA cm^{-2}	Tafel slope (mV dec^{-1})	Reference
np-$Co_9S_4P_4$	Free-standing	1.0 M KOH	40	96	55	This work
np-Co_9S_8	Free-standing	1.0 M KOH	202	271	110	This work
Co_2P nanorods	Ti foil	1.0 M KOH	N/A	152	N/A	Ref. 39
Ni_2P	GCE*	1.0 M KOH	N/A	205	N/A	Ref. 31
CoP	Carbon cloth	1.0 M KOH	N/A	209	129	Ref. 3
FeP NAs NW	Carbon cloth	1.0 M KOH	N/A	218	146	Ref. 5
MoB	GCE*	0.1 M KOH	N/A	225	59	Ref. 40
Porous Mo_2C	GCE*	1.0 M KOH	80	151	59	Ref. 35
$Ni/Ni(OH)_2$	GCE*	0.1M KOH	N/A	300	128	Ref. 41
Ni/NiO/CNT	GCE*	1.0 M KOH	N/A	80	82	Ref. 42
Co/Co_3O_4	Ni foam	1.0 M KOH	30	90	44	Ref. 43
$MoC_{0.654}$@CNS	Ni foam	0.1M KOH	N/A	220	N/A	Ref. 44
Porous Co-based film	Au film	1.0 M KOH	N/A	~375	N/A	Ref. 28
Co-NRCNT	GCE*	1.0 M KOH	N/A	370	N/A	Ref. 10

*GCE: glass carbon electrode

Table S4. Comparison of reported nonprecious metal electrocatalysts for OER in neutral electrolyte. (j: current density; η: overpotential)

Catalysts	Substrate	$j@\eta$=0.57 V (mA cm^{-2})	Tafel slope (mV dec^{-1})	Ref.
np-$Co_9S_4P_4$	Free-standing	25.9	106	This work
np-Co_9S_8	Free-standing	3.12	137	This work
Co-Bi NS/GC	GCE*	14.4	160	Ref. 45
Co-Bi NS	GCE*	5.3	274	Ref. 45
$LiCoPO_4$	GCE*	0.5	120	Ref. 46
Co_3S_4 nanosheets	GCE*	2.4	151	Ref. 47
Co_3O_4/SWNTs	Indium tin oxide (ITO)	6.0	104	Ref. 48
A-$CoS_{4.6}O_{0.6}$ PNCs	GCE*	4.59	164	Ref. 49
Benchmarking RuO2	GCE*	1.79	245	Ref. 49
Co-Pi	GCE*	0.57	74.1	Ref. 50

*GCE: glass carbon electrode

Table S5. Calculated hydrogen adsorption free energy, ΔG_H. The DFT calculations were performed on $Co_9S_{8-x}P_x$. For HER activities, the (001) surfaces are considered as the active surface in the Fm-3m space group structure (The adsorbed H sites in the model are highlighted by red circles).

Compound	Space group	Surface	Structure	site
Co_9S_8	Fm-3m	(001)	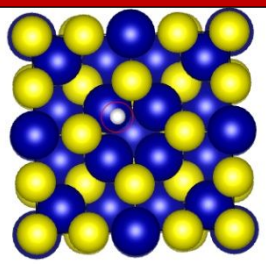	Co
$Co_9S_7P_1$	Fm-3m	(001)	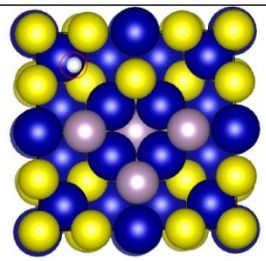	Co
$Co_9S_6P_2$	Fm-3m	(001)	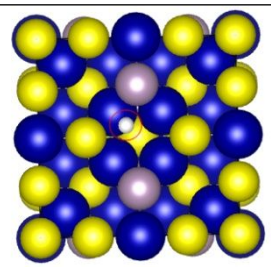	Co
$Co_9S_5P_3$	Fm-3m	(001)	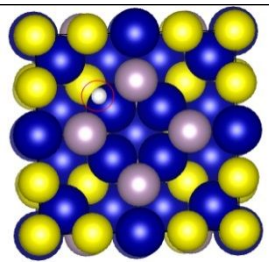	Co
$Co_9S_4P_4$	Fm-3m	(001)	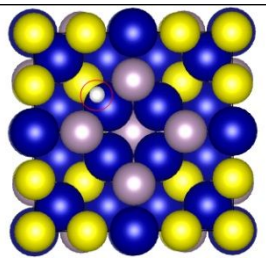	Co

$Co_9S_2P_6$	Fm-3m	(001)	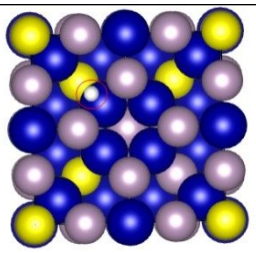	Co

Table S6. The HER kinetic investigation in neutral and basic conditions. Gibbs free energies (G, eV) of adsorbed H_2O, H, and OH on the catalysts; the energy barriers (ΔG, eV) of H_2O dissociation step (Volmer step) and combination of H* into molecular hydrogen (Tafel step) on different catalyst models. Adsorption energy of H is referred to gas phase H_2

Catalysts	G(H) (eV)	G(OH) (eV)	$G(H_2O)$ (eV)	ΔG(H) (eV)	$\Delta G(H_2O)$ (eV)	ΔG(OH+H) (eV)	ΔG(OH) (eV)
Co_9S_8	0.180	-2.971	-1.099	-0.180	1.121	-1.017	-0.718
$Co_9S_6P_2$	0.101	-2.513	-0.637	-0.101	0.899	0.621	0.533
$Co_9S_4P_4$	0.042	-2.409	-0.592	-0.042	0.746	0.542	0.379
$Co_9S_2P_6$	0.073	-2.482	-0.625	-0.073	0.873	0.673	0.412

References

(1) Cobo, S.; Heidkamp, J.; Jacques, P. A.; Fize, J.; Fourmond, V.; Guetaz, L.; Jousselme, B.; Ivanova, V.; Dau, H.; Palacin, S.; Fontecave, M.; Artero, V., A Janus cobalt-based catalytic material for electro-splitting of water. *Nat. Mater.* **2012**, 11 (9), 802-807.

(2) Sun, Y.; Liu, C.; Grauer, D. C.; Yano, J.; Long, J. R.; Yang, P.; Chang, C. J., Electrodeposited cobalt-sulfide catalyst for electrochemical and photoelectrochemical hydrogen generation from water. *J. Am. Chem. Soc.* **2013**, 135 (47), 17699-17702.

(3) Tian, J.; Liu, Q.; Asiri, A. M.; Sun, X., Self-supported nanoporous cobalt phosphide nanowire arrays: an efficient 3D hydrogen-evolving cathode over the wide range of pH 0-14. *J. Am. Chem. Soc.* **2014**, 136 (21), 7587-7590.

(4) Pu, Z.; Liu, Q.; Jiang, P.; Asiri, A. M.; Obaid, A. Y.; Sun, X., CoP Nanosheet Arrays Supported on a Ti Plate: An Efficient Cathode for Electrochemical Hydrogen Evolution. *Chem. Mater.* **2014**, 26 (15), 4326-4329.

(5) Liang, Y.; Liu, Q.; Asiri, A. M.; Sun, X.; Luo, Y., Self-Supported FeP Nanorod Arrays: A Cost-Effective 3D Hydrogen Evolution Cathode with High Catalytic Activity. *ACS Catal.* **2014**, 4 (11), 4065-4069.

(6) Juan F. Callejas, J. M. M., Carlos G. Read, J. Chance Crompton, Adam J. Biacchi, Eric J. Popczun, Thomas R. Gordon, Nathan S. Lewis, and Raymond E. Schaak, Electrocatalytic and Photocatalytic Hydrogen Production from Acidic and Neutral-pH Aqueous Solutions Using Iron Phosphide Nanoparticles. *ACS Nano* **2014**, 8 (11), 11101-11107.

(7) Xing, Z.; Liu, Q.; Asiri, A. M.; Sun, X., High-Efficiency Electrochemical Hydrogen Evolution Catalyzed by Tungsten Phosphide Submicroparticles. *ACS Catal.* **2014**, 5 (1), 145-149.

(8) Cui, W.; Liu, Q.; Xing, Z.; Asiri, A. M.; Alamry, K. A.; Sun, X., MoP nanosheets supported on biomass-derived carbon flake: One-step facile preparation and application as a novel high-active electrocatalyst toward hydrogen evolution reaction. *Appl. Catal. B-Environ.* **2015**, 164, 144-150.

(9) Feng, L. L.; Li, G. D.; Liu, Y.; Wu, Y.; Chen, H.; Wang, Y.; Zou, Y. C.; Wang, D.; Zou, X., Carbon-armored Co_9S_8 nanoparticles as all-pH efficient and durable H2-evolving electrocatalysts. *ACS Appl. Mater. Interfaces* **2015**, 7 (1), 980-988.

(10) Zou, X.; Huang, X.; Goswami, A.; Silva, R.; Sathe, B. R.; Mikmekova, E.; Asefa, T., Cobalt-embedded nitrogen-rich carbon nanotubes efficiently catalyze hydrogen evolution reaction at all pH values. *Angew. Chem. Int. Ed.* **2014**, 53 (17), 4372-4376.

(11) Liang, H. W.; Bruller, S.; Dong, R.; Zhang, J.; Feng, X.; Mullen, K., Molecular metal-Nx centres in porous carbon for electrocatalytic hydrogen evolution. *Nat. Commun.* **2015**, 6, 7992.

(12) Feng, L. L.; Yu, G.; Wu, Y.; Li, G. D.; Li, H.; Sun, Y.; Asefa, T.; Chen, W.; Zou, X., High-index faceted Ni_3S_2 nanosheet arrays as highly active and ultrastable electrocatalysts for water splitting. *J. Am. Chem. Soc.* **2015**, 137 (44), 14023-14026.

(13) Jiang, N.; Bogoev, L.; Popova, M.; Gul, S.; Yano, J.; Sun, Y., Electrodeposited nickel-sulfide films as competent hydrogen evolution catalysts in neutral water. *J. Mater. Chem. A* **2014**, 2 (45), 19407-19414.

(14) Merki, D.; Fierro, S.; Vrubel, H.; Hu, X., Amorphous molybdenum sulfide films as catalysts for electrochemical hydrogen production in water. *Chem. Sci.* **2011**, 2 (7), 1262-1267.

(15) Ge, X.; Chen, L.; Zhang, L.; Wen, Y.; Hirata, A.; Chen, M., Nanoporous metal enhanced catalytic activities of amorphous molybdenum sulfide for high-efficiency hydrogen production. *Adv. Mater.* **2014**, 26 (19), 3100-3104.

(16) Jianwei Miao; Fang-Xing Xiao; Hong Bin Yang; Si Yun Khoo; Jiazang Chen; Zhanxi Fan; Ying-Ya Hsu; Hao Ming Chen; Hua Zhang; Liu, B., Hierarchical Ni-Mo-S nanosheets on carbon fiber cloth: A flexible electrode for efficient hydrogen generation in neutral electrolyte. *Sci. Adv.* **2015**, 1, e1500259.

(17) Hou, Y.; Zhang, B.; Wen, Z.; Cui, S.; Guo, X.; He, Z.; Chen, J., A 3D hybrid of layered MoS_2/nitrogen-doped graphene nanosheet aerogels: an effective catalyst for hydrogen evolution in microbial electrolysis cells. *J. Mater. Chem. A* **2014**, 2 (34), 13795-13800.

(18) Tran, P. D.; Nguyen, M.; Pramana, S. S.; Bhattacharjee, A.; Chiam, S. Y.; Fize, J.; Field, M. J.; Artero, V.; Wong, L. H.; Loo, J.; Barber, J., Copper molybdenum sulfide: a new efficient electrocatalyst for hydrogen production from water. *Energy Environ. Sci.* **2012**, 5 (10), 8912-8916.

(19) Liu, Y.; Yu, G.; Li, G. D.; Sun, Y.; Asefa, T.; Chen, W.; Zou, X., Coupling Mo_2C with Nitrogen-Rich Nanocarbon Leads to Efficient Hydrogen-Evolution Electrocatalytic Sites. *Angew. Chem. Int. Ed.* **2015**, 54 (37), 10752-10757.

(20) Valenti, G.; Boni, A.; Melchionna, M.; Cargnello, M.; Nasi, L.; Bertoni, G.; Gorte, R. J.; Marcaccio, M.; Rapino, S.; Bonchio, M.; Fornasiero, P.; Prato, M.; Paolucci, F., Co-axial heterostructures integrating palladium/titanium dioxide with carbon nanotubes for efficient electrocatalytic hydrogen evolution. *Nat. Commun.* **2016**, 7, 13549.

(21) Kong, D.; Cha, J. J.; Wang, H.; Lee, H. R.; Cui, Y., First-row transition metal dichalcogenide catalysts for hydrogen evolution reaction. *Energy Environ. Sci.* **2013**, 6 (12), 3553-3558.

(22) Kong, D.; Wang, H.; Lu, Z.; Cui, Y., $CoSe_2$ nanoparticles grown on carbon fiber paper: an efficient and stable electrocatalyst for hydrogen evolution reaction. *J. Am. Chem. Soc.* **2014**, 136 (13), 4897-4900.

(23) Peng, S.; Li, L.; Han, X.; Sun, W.; Srinivasan, M.; Mhaisalkar, S. G.; Cheng, F.; Yan, Q.; Chen, J.; Ramakrishna, S., Cobalt sulfide nanosheet/graphene/carbon nanotube nanocomposites as flexible electrodes for hydrogen evolution. *Angew. Chem. Int. Ed.* **2014**, 53 (46), 12594-12599.

(24) Wang, D. Y.; Gong, M.; Chou, H. L.; Pan, C. J.; Chen, H. A.; Wu, Y.; Lin, M. C.; Guan, M.; Yang, J.; Chen, C. W.; Wang, Y. L.; Hwang, B. J.; Chen, C. C.; Dai, H., Highly active and stable hybrid catalyst of cobalt-doped FeS_2 nanosheets-carbon nanotubes for hydrogen evolution reaction. *J. Am. Chem. Soc.* **2015**, 137 (4), 1587-1592.

(25) Faber, M. S.; Dziedzic, R.; Lukowski, M. A.; Kaiser, N. S.; Ding, Q.; Jin, S., High-performance electrocatalysis using metallic cobalt pyrite (CoS_2) micro- and nanostructures. *J. Am. Chem. Soc.* **2014**, 136 (28), 10053-10061.

(26) Kibsgaard, J.; Chen, Z.; Reinecke, B. N.; Jaramillo, T. F., Engineering the surface structure of MoS_2 to preferentially expose active edge sites for electrocatalysis. *Nat. Mater.* **2012**, 11 (11), 963-969.

(27) Callejas, J. F.; Read, C. G.; Popczun, E. J.; McEnaney, J. M.; Schaak, R. E., Nanostructured Co_2P Electrocatalyst for the Hydrogen Evolution Reaction and Direct Comparison with Morphologically Equivalent CoP. *Chem. Mater.* **2015**, 27 (10), 3769-3774.

(28) Yang, Y.; Fei, H.; Ruan, G.; Tour, J. M., Porous cobalt-based thin film as a bifunctional catalyst for hydrogen generation and oxygen generation. *Adv. Mater.* **2015**, 27 (20), 3175-3180.

(29) Liu, Q.; Tian, J.; Cui, W.; Jiang, P.; Cheng, N.; Asiri, A. M.; Sun, X., Carbon nanotubes decorated with CoP nanocrystals: a highly active non-noble-metal nanohybrid electrocatalyst for hydrogen evolution. *Angew. Chem. Int. Ed.* **2014**, 53 (26), 6710-6714.

(30) Popczun, E. J.; Read, C. G.; Roske, C. W.; Lewis, N. S.; Schaak, R. E., Highly active electrocatalysis of the hydrogen evolution reaction by cobalt phosphide nanoparticles. *Angew. Chem. Int. Ed.* **2014**, 53 (21), 5427-5430.

(31) Popczun, E. J.; McKone, J. R.; Read, C. G.; Biacchi, A. J.; Wiltrout, A. M.; Lewis, N. S.; Schaak, R. E., Nanostructured nickel phosphide as an electrocatalyst for the hydrogen evolution reaction. *J. Am. Chem. Soc.* **2013**, 135 (25), 9267-9270.

(32) Tian, J.; Liu, Q.; Cheng, N.; Asiri, A. M.; Sun, X., Self-supported Cu_3P nanowire arrays as an integrated high-performance three-dimensional cathode for generating hydrogen from water. *Angew. Chem. Int. Ed.* **2014**, 53 (36), 9577-9581.

(33) Xing, Z.; Liu, Q.; Asiri, A. M.; Sun, X., Closely interconnected network of molybdenum phosphide nanoparticles: a highly efficient electrocatalyst for generating hydrogen from water. *Adv. Mater.* **2014**, 26 (32), 5702-5707.

(34) Yan, H.; Tian, C.; Wang, L.; Wu, A.; Meng, M.; Zhao, L.; Fu, H., Phosphorus-modified tungsten nitride/reduced graphene oxide as a high-performance, non-noble-metal electrocatalyst for the hydrogen evolution reaction. *Angew. Chem. Int. Ed.* **2015**, 54 (21), 6325-6329.

(35) Wu, H. B.; Xia, B. Y.; Yu, L.; Yu, X. Y.; Lou, X. W., Porous molybdenum carbide nano-octahedrons synthesized via confined carburization in metal-organic frameworks for efficient hydrogen production. *Nat. Commun.* **2015**, 6, 6512.

(36) Kibsgaard, J.; Jaramillo, T. F., Molybdenum phosphosulfide: an active, acid-stable, earth-abundant catalyst for the hydrogen evolution reaction. *Angew. Chem. Int. Ed.* **2014**, 53 (52), 14433-14437.

(37) Caban-Acevedo, M.; Stone, M. L.; Schmidt, J. R.; Thomas, J. G.; Ding, Q.; Chang, H. C.; Tsai, M. L.; He, J. H.; Jin, S., Efficient hydrogen evolution catalysis using ternary pyrite-type cobalt phosphosulphide. *Nat. Mater.* **2015**, 14 (12), 1245-1251.

(38) Ye, R.; del Angel-Vicente, P.; Liu, Y.; Arellano-Jimenez, M. J.; Peng, Z.; Wang, T.; Li, Y.; Yakobson, B. I.; Wei, S. H.; Yacaman, M. J.; Tour, J. M., High-Performance Hydrogen Evolution from $MoS_{2(1-x)}$ $P_{(x)}$ Solid Solution. *Adv. Mater.* **2016**, 28 (7), 1427-1432.

(39) Huang, Z.; Chen, Z.; Chen, Z.; Lv, C.; Humphrey, M. G.; Zhang, C., Cobalt phosphide nanorods as an efficient electrocatalyst for the hydrogen evolution reaction. *Nano Energy* **2014**, 9, 373-382.

(40) Vrubel, H.; Hu, X., Molybdenum boride and carbide catalyze hydrogen evolution in both acidic and basic solutions. *Angew. Chem. Int. Ed.* **2012**, 51 (51), 12703-12706.

(41) Danilovic, N.; Subbaraman, R.; Strmcnik, D.; Chang, K. C.; Paulikas, A. P.; Stamenkovic, V. R.; Markovic, N. M., Enhancing the alkaline hydrogen evolution reaction activity through the bifunctionality of $Ni(OH)_2$/metal catalysts. *Angew. Chem. Int. Ed.* **2012**, 51 (50), 12495-12498.

(42) Gong, M.; Zhou, W.; Tsai, M. C.; Zhou, J.; Guan, M.; Lin, M. C.; Zhang, B.; Hu, Y.; Wang, D. Y.; Yang, J.; Pennycook, S. J.; Hwang, B. J.; Dai, H., Nanoscale nickel oxide/nickel heterostructures for active hydrogen evolution electrocatalysis. *Nat. Commun.* **2014**, 5, 4695.

(43) Yan, X.; Tian, L.; He, M.; Chen, X., Three-Dimensional Crystalline/Amorphous Co/Co_3O_4 Core/Shell Nanosheets as Efficient Electrocatalysts for the Hydrogen Evolution Reaction. *Nano Lett.* **2015**, 15 (9), 6015-6021.

(44) Zhu, J.; Sakaushi, K.; Clavel, G.; Shalom, M.; Antonietti, M.; Fellinger, T. P., A general salt-templating method to fabricate vertically aligned graphitic carbon nanosheets and their metal carbide hybrids for superior lithium ion batteries and water splitting. *J. Am. Chem. Soc.* **2015**, 137 (16), 5480-5485.

(45) Chen, P.; Xu, K.; Zhou, T.; Tong, Y.; Wu, J.; Cheng, H.; Lu, X.; Ding, H.; Wu, C.; Xie, Y., Strong-Coupled Cobalt Borate Nanosheets/Graphene Hybrid as Electrocatalyst for Water Oxidation Under Both Alkaline and Neutral Conditions. *Angew. Chem. Int. Ed.* 2016, 55 (7), 2488-2492.

(46) Lee, S. W.; Carlton, C.; Risch, M.; Surendranath, Y.; Chen, S.; Furutsuki, S.; Yamada, A.; Nocera, D. G.; Shao-Horn, Y., The nature of lithium battery materials under oxygen evolution reaction conditions. *J. Am. Chem. Soc.* **2012**, 134 (41), 16959-16962.

(47) Liu, Y.; Xiao, C.; Lyu, M.; Lin, Y.; Cai, W.; Huang, P.; Tong, W.; Zou, Y.; Xie, Y., Ultrathin Co_3S_4 nanosheets that synergistically engineer spin states and exposed polyhedra that promote water oxidation under neutral conditions. *Angew. Chem. Int. Ed.* **2015**, 54 (38), 11231-11235.

(48) Wu, J.; Xue, Y.; Yan, X.; Yan, W.; Cheng, Q.; Xie, Y., Co_3O_4 nanocrystals on single-walled carbon nanotubes as a highly efficient oxygen-evolving catalyst. *Nano Res.* **2012**, 5 (8), 521-530.

(49) Cai, P.; Huang, J.; Chen, J.; Wen, Z., Oxygen-Containing Amorphous Cobalt Sulfide Porous Nanocubes as High-Activity Electrocatalysts for the Oxygen Evolution Reaction in an Alkaline/Neutral Medium. *Angew. Chem. Int. Ed.* **2017**, 56 (17), 4858-4861.

(50) Ahn, H. S.; Tilley, T. D., Electrocatalytic Water Oxidation at Neutral pH by a Nanostructured $Co(PO_3)_2$ Anode. *Adv. Funct. Mater.* **2013**, 23 (2), 227-233.